A STUDY ON RAMAN INJECTION LASER

A Thesis

by

DEBIN LIU

Submitted to the Office of Graduate Studies of
Texas A&M University
in partial fulfillment of the requirements for the degree of

MASTER OF SCIENCE

August 2005

Major Subject: Physics

A STUDY ON RAMAN INJECTION LASER

A Thesis

by

DEBIN LIU

Submitted to the Office of Graduate Studies of
Texas A&M University
in partial fulfillment of the requirements for the degree of

MASTER OF SCIENCE

Approved by:

Chair of Committee,	Alexey Belyanin
Committee Members,	Olga Kocharovskaya
	Philip Hemmer
Head of Department,	Edward Fry

August 2005

Major Subject: Physics

ABSTRACT

A Study on Raman Injection Laser.

(August 2005)

Debin Liu,

B.S., University of Science & Technology of China

Chair of Advisory Committee: Dr. Alexey Belyanin

The Raman Injection Laser is a new type of laser which is based on triply resonant stimulated Raman scattering between quantum confined states within the active region of a Quantum Cascade Laser that serves as an internal optical pump. The Raman Injection Laser is driven electrically and no external laser pump is required. Triple resonance leads to an enhancement of orders of magnitude in the Raman gain, high conversion efficiency and low threshold. We studied this new type of laser and conclude some basic equations. With reasonable experimental parameters, we calculated the laser gain, losses and the output power of the Raman Injection Laser by using Mathematica and FEMLab. Finally we compared the theoretical and experimental results.

DEDICATION

To my parents

ACKNOWLEDGEMENTS

I feel very fortunate to have had the opportunity to study and carry out research from Professor Alexey Belyanin. I would like to thank him for his guidance, encouragement and support throughout the study of this research.

I also would like to thank Feng Xie for his kindness in helping me with the questions I encountered during my study.

I also would like to thank Professor Kocharovskaya and Professor Hemmer for their patience and support.

Thanks also to my friends and colleagues and the department faculty and staff for making my time at Texas A&M University a great experience.

Finally, thanks to my mother and father for their encouragement and love.

TABLE OF CONTENTS

Page

LIST OF FIGURES

INTRODUCTION

Stimulated Raman scattering is a nonlinear optical process that, in a broad variety of materials, enables the generation of optical gain at a frequency that is shifted from that of the incident radiation by an amount corresponding to the frequency of an internal oscillation of the material. This effect is the basis for a broad class of tunable sources known as Raman lasers. In general, these sources have only a small gain and therefore require external pumping with powerful lasers, which limits their applications [1].

A Quantum Cascade Laser operates due to population inversion on the intersubband transition between quantum confined electron states in semiconductor quantum well structures. In this structure, the typical lasing scheme of a Quantum Cascade Laser is 4-level scheme in Fig. 2.

Recently, the Raman Injection Laser was developed. The Raman Injection Laser represents several key innovations in laser technology, combining the advantages of nonlinear optical devices and the Quantum Cascade Laser with a compact design.

The physics underlying the Raman Injection Laser differs in a fundamental way from the existing Raman lasers. The Raman Injection Laser is based on triply resonant stimulated Raman scattering between quantum confined states within the active

---

This thesis follows the style of Physical Review D.

region of a Quantum Cascade Laser that serves as an internal optical pump.

The Raman Injection Laser is driven electrically and no external laser pump is required. This leads to an enhancement of orders of magnitude in the Raman gain, high conversion efficiency and low threshold [1].

The theoretical design and analysis of the Raman Injection Laser are based on Maxwell's equations and density-matrix equations.

In this thesis, we first introduce the Quantum Cascade Laser and the Raman laser. We show how the Raman Injection Laser combines the advantages of these two lasers. Then starting from the Maxwell's equations and density-matrix equations, we conclude the basic equations for the lasing system of the Raman Injection Laser. And using reasonable parameters from experiment, we calculate laser gain, losses and power by computer. Finally we compare our theoretical power curves with the experiment measurement.

QUANTUM CASCADE LASER

The Quantum Cascade Lasers were invented and first demonstrated in 1994. They have already reached a remarkably high level of maturity.

A Quantum Cascade Laser is a sliver of semiconductor material about the size of a tick. Inside, electrons are constrained within layers of gallium and aluminum compounds, called quantum wells that are nanometers thick. In such a tight space, electrons take on properties explained by quantum physics.

In the conventional lasers, Fig. 1, a photon of light is emitted when a negative charge (an electron) jumps from a semiconductor's conduction band to a positive charge (or "hole") in the valence band. Once an electron has been neutralized by a hole, it can emit no more photons.

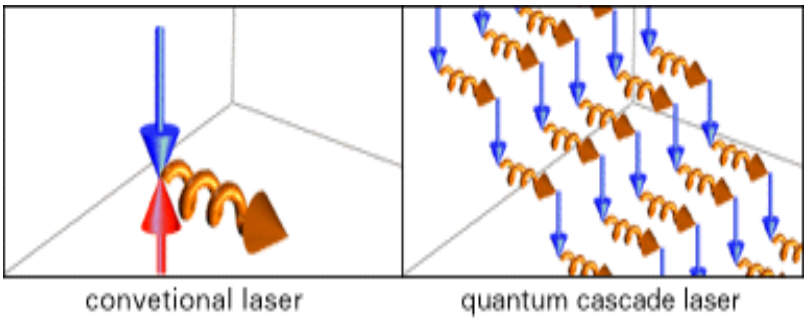

FIG. 1. Lasing process.

A Quantum Cascade Laser contains a series of quantum wells and operates like an electronic waterfall. Electrons cascade down a series of identical energy steps, emitting a photon and losing energy at each step.

The Quantum Cascade Laser operates due to population inversion on the intersubband transition between quantum-confined electron states in semiconductor quantum-well structures. They utilize a typical 4-level lasing scheme in Fig. 2, in which electrons are injected to the upper laser state 3 from the upstream injector 4 by resonant tunneling, make radiative or nonradiative transition to the lower laser state 2, and then rapidly depopulate this state via phonon emission and tunneling out of the active region to the injector section downstream. This section serves as an upstream injector for the next active stage [2].

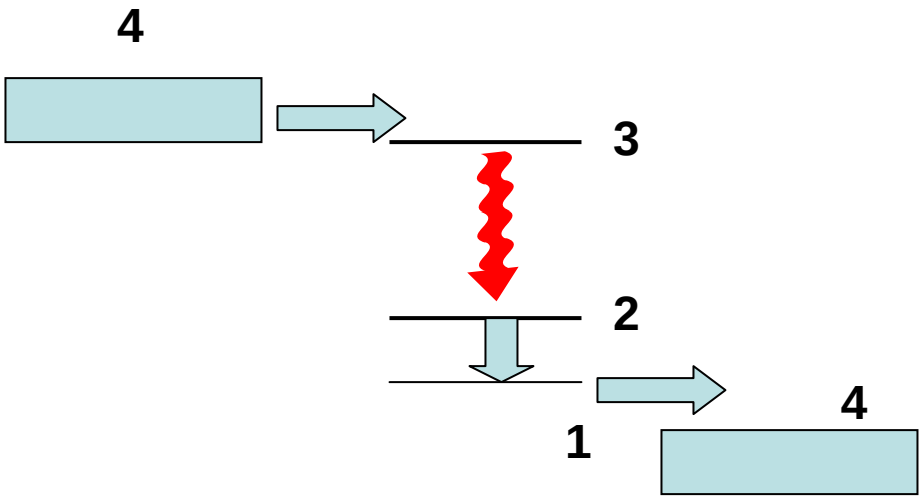

FIG. 2. 4-level lasing scheme.

When the lower-energy electron leaves the first well, it enters a region of material, level 4 in Fig. 2, where it is collected and sent to the next well, Fig. 3. Typically 25 to 75 active wells are arranged in a QC laser, each at a slightly lower energy level than the one before, thus producing the cascade effect, and allowing 25 to 75 photons to be created per electron journey.

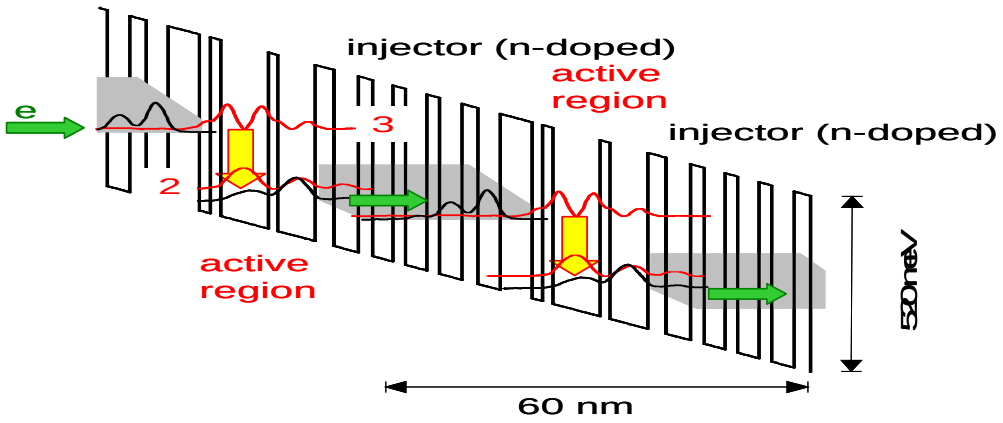

FIG. 3. Cascading structure in a Quantum Cascade Laser.

Clearly, the cascading structure of the Quantum Cascade Laser has unique efficiency in controlling electron transport, lifetimes and populations of electron states in combination with flexibility of the active region design [3].

Also because of the similar effective masses, different subbands have similar

dispersion. Therefore, there is no cross-absorption between intersubband transitions at different frequencies in the cascading structure of a Quantum Cascade Laser.

RAMAN LASER

When light is scattered from a molecule, most photons are elastically scattered. The scattered photons have the same energy and, therefore, wavelength, as the incident photons. However, a small fraction of light is scattered at optical frequencies different from, and usually lower than, the frequency of the incident photons. The process leading to this inelastic scattering is termed the Raman Effect. Raman scattering can occur with a change in the vibrational, rotational or electronic energy of a molecule.

If the molecule of the medium changes its energy state and the photon loses an equivalent energy, the scattered light has a lower frequency and is called the Stokes radiation, Fig. 4.

$$\omega_S = \omega_L - \omega_R.$$

If a molecule is in an excited state, the reverse scattering process can take place. In that case, the scattered light has a higher frequency than the exciting light and is called the anti-Stokes radiation, Fig. 4.

$$\omega_{AS} = \omega_L + \omega_R.$$

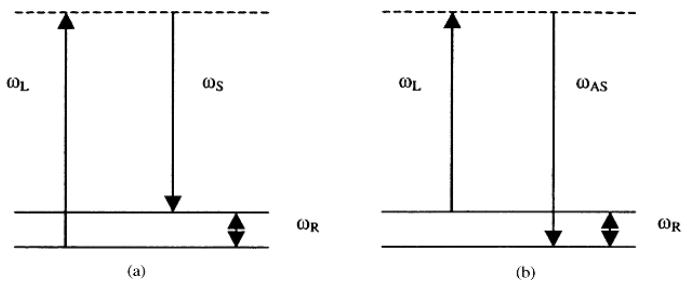

FIG. 4. Stokes and anti-Stokes Raman scattering. (a) Stokes, (b)anti-Stokes.

The stimulated Raman scattering is a two photon nonlinear optical process that, in a broad variety of materials, enables the generation of optical gain at a frequency that is shifted from that of the incident radiation by an amount corresponding to the frequency of an internal oscillation of the material1. This effect is the basis for a broad class of tunable sources known as Raman lasers.

The Raman Laser works as follows: Light hits a substance, causing the atoms in the substance to vibrate sympathetically. The collision of photons with the substance causes some of the photons to gain or lose energy, resulting in a scattered light of a different wavelength. A Raman laser essentially involves taking this scattered light and then amplifying it by reflecting it and pumping energy into the system to emit a coherent laser beam.

The Raman Lasers have typically small gain (10^{-9} cm/W) and therefore require a large and powerful external pump to compensate for the beam's attenuation, or

weakening, as it propagates through the material, which limits their applications [1].

RAMAN INJECTION LASER

To circumvent these limitations of traditional Raman laser, the Raman Injection Laser is developed, Fig. 5. The Raman Injection Laser is based on triply resonant stimulated Raman scattering between quantum confined states within the active region of a Quantum Cascade Laser that serves as an internal optical pump.

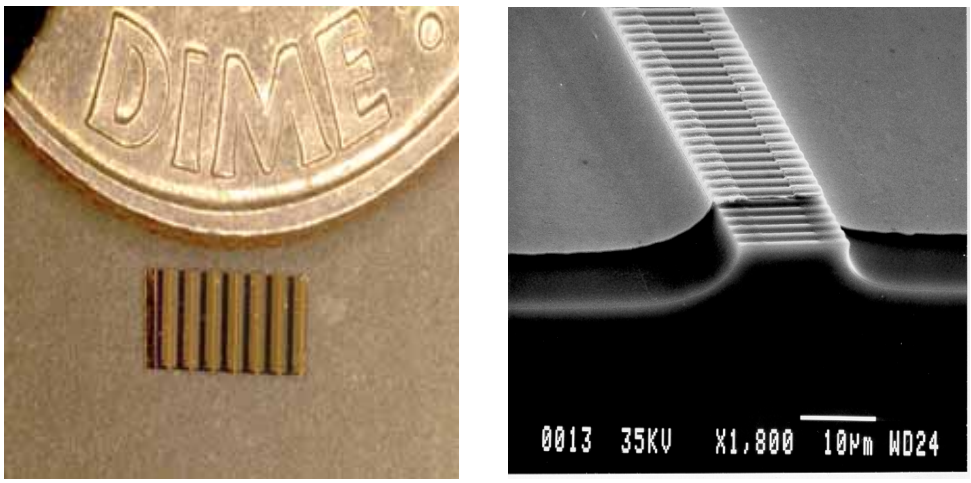

FIG. 5. Size of the Raman Injection Laser. width 3-15 μm, length 1-3 mm.

The main idea of the Raman Injection Laser is to monolithically integrate active laser medium and the nonlinear medium in such a way that the laser field could serve as an intracavity optical pump for the desired nonlinear optical interaction [3].

The active nonlinear systems support both laser action and, at the same time, nonlinear self-conversion of laser light into coherent radiation at different frequencies. With application to intersubband transitions, the nonlinear section, a coupled quantum well containing a desired set of intersubband transitions, is incorporated into an active region of a Quantum Cascade Laser.

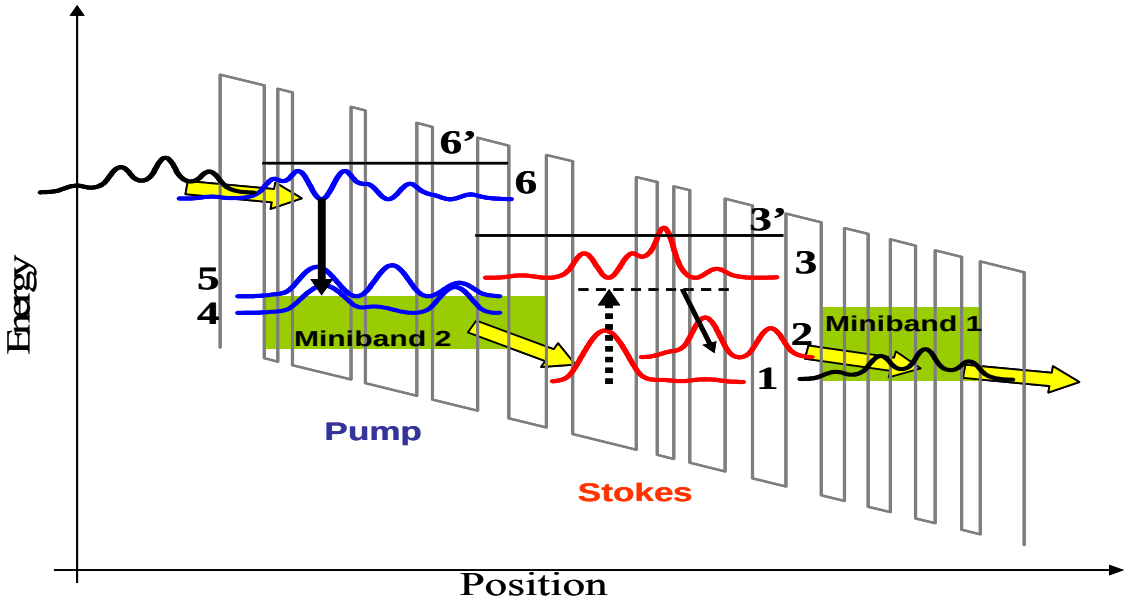

FIG. 6. Raman structure. The Raman Injection Laser monolithically integrated with its own optical pump. Active region of a resonant Raman laser integrates fundamental laser cascade 6-5-4 and resonant Λ-scheme of transitions 1-3-2-1 for Raman Stokes lasing.

In the waveguide core of the Raman Injection Laser, there are 30 repetitions of active region and Raman Structure. The Fig. 6 represents one period of this structure.

The yellow arrows indicate the direction of electron transport. The solid and dashed vertical arrows represent the internally generated pump laser radiation.

Laser light at 6.7 μm generated on the transition 6-5 serves as a resonant optical pump for lasing at the Stokes wavelength of 9 μm, which is detuned by 15 meV from the transition 3-2. Resonant absorption of the pump at the transition 1-3 is overcome by amplification in the pump laser section at the transition 6-5. Electrons in the state 1 are injected into the state 6 of the following period.

The Raman Injection Laser is driven electrically and no external laser pump is required. Triple resonance leads to an enhancement of orders of magnitude in the Raman gain. It approaches 10^{-3} cm/W (10^{6} times higher than in existing Raman lasers), high conversion efficiency (30%) and low threshold [1].

THEORY

The analysis of the Raman Injection Laser is based on coupled density-matrix equations and Maxwell's equations. We assume that the electromagnetic field is classical and is described by Maxwell's equations.

Density-matrix equations

Since we are dealing with resonant optical nonlinearities, the natural way to treat the interaction of light with electron subsystem is through the density matrix equations. It allows one to easily incorporate many interacting fields and various incoherent relaxation and scattering processes.

We first start from the simplest 3-level system, Fig. 7:

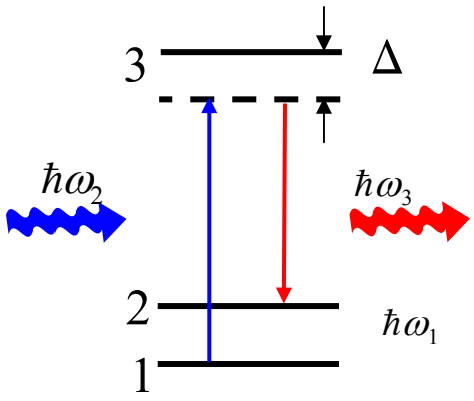

FIG. 7. 3-level system.

The Hamiltonian of this system is $H=H_0+H_{int}$.

where

$$H_0 = \hbar\omega_1|1\rangle\langle 1| + \hbar\omega_2|2\rangle\langle 2| + \hbar\omega_3|3\rangle\langle 3|$$

$$H_{int} = -\hbar\left(\Omega_1 e^{-\nu_1 t}|2\rangle\langle 1| + \Omega_2 e^{-\nu_2 t}|3\rangle\langle 1| + \Omega_3 e^{-\nu_3 t}|3\rangle\langle 2| + c.c\right)$$

The $\Omega = \frac{d\varepsilon}{2\hbar}$ is the Rabi frequency. d is the dipole moment. ε is the slowly varying complex amplitude of field. ν is the wave frequency.

The total Hamiltonian includes a system of electron states and its coherent interaction with electromagnetic field, while all relaxation and scattering processes are considered as the decay-term.

We proceed with several important approximations: 1, we neglect most many-body effects due to the Coulomb interaction of electrons. 2, we neglect the effect of the laser field on the electron wavefunctions and dipole moments of the ISB transitions. 3, in evaluating the dynamics of populations (diagonal terms in the density matrix), we replace the realistic spatial kinetics of electron transport through the structure with rate equations for a set of electron states, with the transition times between different states defined by phonon emission and tunneling.

Then simply we start from the dynamics:

$$\frac{\partial \rho_{ij}}{\partial t} = -\frac{i}{\hbar}\left[H,\rho_{ij} \right] + decayterm \qquad (1)$$

where the ρ are the density matrix elements.

$$i\hbar \frac{\partial \rho_{ij}}{\partial t} = \sum_k \left(H_{ik}\rho_{kj} - \rho_{ik}H_{kj} \right) + decayterm$$

Plug in the expression of $H=H_0+H_{int}$, and consider the relaxing time for the decay-term. We get the density matrix equations of diagonal elements for this 3-level system:

$$dn_1/dt = -2\,\mathrm{Im}[\Omega_1^*\sigma_{21}] - 2\,\mathrm{Im}[\Omega_2^*\sigma_{31}] + r_{21}n_2 + r_{31}n_3$$

$$dn_2/dt = 2\,\mathrm{Im}[\Omega_1^*\sigma_{21}] - 2\,\mathrm{Im}[\Omega_3^*\sigma_{32}] + r_{32}n_3 - r_{21}n_2$$

$$dn_3/dt = 2\,\mathrm{Im}[\Omega_2^*\sigma_{31}] + 2\,\mathrm{Im}[\Omega_3^*\sigma_{32}] - (r_{31}+r_{32})n_3$$

Considering only the slow varying part of off-diagonal element, we replace the off-diagonal elements of the density matrix as:

$$\rho_{ij}(t) = \sigma_{ij}(t)e^{-i\nu_j t}$$

We get the equations of off-diagonal elements:

$$d\sigma_{21}/dt + \Gamma_{21}\sigma_{21} = i\Omega_1 n_{12} - i\Omega_2\sigma_{32}^* + i\Omega_3^*\sigma_{31}$$

$$d\sigma_{31}/dt + \Gamma_{31}\sigma_{31} = i\Omega_2 n_{13} - i\Omega_1\sigma_{32} + i\Omega_3\sigma_{21}$$

$$d\sigma_{32}/dt + \Gamma_{32}\sigma_{32} = i\Omega_3 n_{23} - i\Omega_1^*\sigma_{31} + i\Omega_2\sigma_{21}^*$$

Where the $\Gamma_{ij} = \gamma_{ij}+i\Delta_{ij}$. $\Delta_{ij} = \omega_{ij}-\nu_j = \omega_i-\omega_j-\nu_j$ is the detuning of corresponding transitions. $n_{ij} = \rho_{ii}-\rho_{jj}$ is the difference of populations of corresponding energy levels. σ_{jk} is the slowly varying amplitude of the corresponding elements. r_{ij} is the relaxation rates of transitions i to j. $n_i = \rho_{ii}$ [4].

Our system is more complicated than the above three-level system. It includes, as a minimum, states 1, 2, 3, 5 and 6 coupled by two laser fields. We assume that the injector states remain undepleted and do not need to be included directly. Also, our system is an open system. This means that the sum of populations of states 1, 2, and 3 is not conserved and one can control them quite efficiently by combination of scattering and tunneling processes.

Then we ignore the field Ω_1 which is between level 1 and 2, and we get the density-matrix equations.

For off-diagonal elements:

$$\frac{d\sigma_{21}}{dt}+\Gamma_{21}\sigma_{21}=-i\Omega_2\sigma_{32}^{*}+i\Omega_3^{*}\sigma_{31}$$

$$\frac{d\sigma_{32}}{dt}+\Gamma_{32}\sigma_{32}=i\Omega_3 n_{23}+i\Omega_2\sigma_{21}^{*}$$

$$\frac{d\sigma_{31}}{dt}+\Gamma_{31}\sigma_{31}=i\Omega_2 n_{13}+i\Omega_3\sigma_{21}$$

$$\frac{d\sigma_{65}}{dt}+\Gamma_{65}\sigma_{65}=i\Omega_2 n_{65}$$

For diagonal elements:

$$\frac{\partial n_1}{\partial t}=j_1+r_{31}n_3+r_{21}n_2-r_{12}n_1-r_1(n_1-n_{1T})-2\,\mathrm{Im}\left[\sigma_{31}\Omega_2^{*}\right]$$

$$\frac{\partial n_2}{\partial t}=j_2+r_{32}n_3+r_{12}n_1-r_{21}n_2-r_2(n_2-n_{2T})-2\,\mathrm{Im}\left[\sigma_{32}\Omega_3^{*}\right]$$

$$\frac{\partial n_3}{\partial t}=-r_3 n_3+2\,\mathrm{Im}\left[\sigma_{32}\Omega_3^{*}\right]+2\,\mathrm{Im}\left[\sigma_{31}\Omega_2^{*}\right]$$

$$\frac{\partial n_5}{\partial t}=j(1-\eta)+r_{65}n_5-r_5(n_5-n_{5T})-2\,\mathrm{Im}\left[\sigma_{65}\Omega_2^{*}\right]$$

$$\frac{\partial n_6}{\partial t}=j\eta-r_6 n_6+2\,\mathrm{Im}\left[\sigma_{65}\Omega_2^{*}\right]$$

Here j is the total current density, $j_{1,2}$ are the densities of current flowing through the states 1 and 2. We will assume that $j_1 + j_2 = j$. The factor η is the efficiency of injection to the upper drive laser state 6; we again assume that the rest of the current goes to state 5. Because of relative higher state energy, equilibrium populations of states 3 and 6 are neglected.

The relaxation rate r_i is the inverse time during which state i reaches equilibrium with the injector; we assume that the injector remains undepleted and has Fermi distribution of electrons at temperature T. The relaxation rate r_{ij} is the inverse time of the transition from state i to state j.

Maxwell's equations

For ISB transitions close to the Γ-point in the conduction band, the dipole moments only have z-components, as indicated in Fig. 8. Therefore, TM-polarized modes with a large z-component of the electric field are preferentially excited.

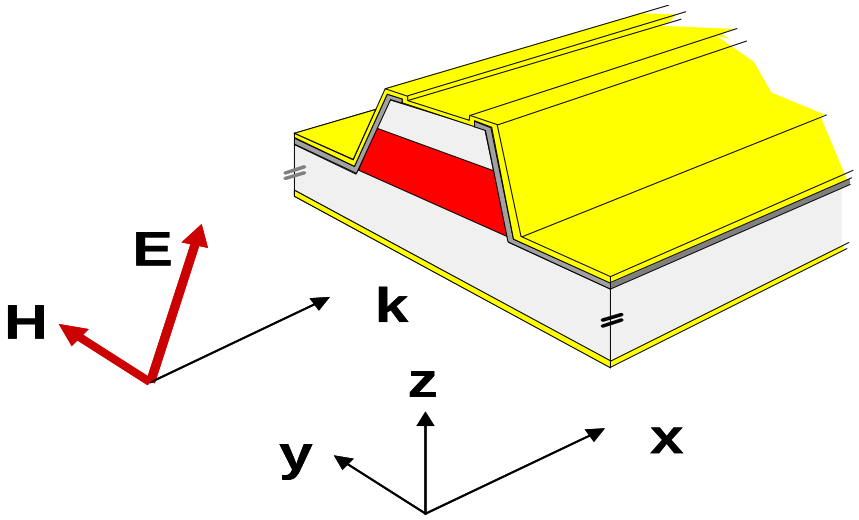

FIG. 8. Geometry of the Raman Injection Laser.

In the Maxwell's equations it is convenient to separate resonant ISB polarization **P** from non-resonant dielectric response described by the complex dielectric function $\varepsilon(x, y, z)$ as follows:

$$\nabla \times \mathbf{H} = \frac{\varepsilon}{c}\frac{\partial \mathbf{E}}{\partial t} + \frac{4\pi}{c}\frac{\partial \mathbf{P}}{\partial t}$$

$$\nabla \times \mathbf{E} = -\frac{1}{c}\frac{\partial \mathbf{H}}{\partial t}$$

In the simplest case of a plane-parallel semiconductor waveguide, the dielectric function has a piecewise-constant profile in z-direction and is constant in y-direction, with jumps on the lateral walls of the waveguide.

Combine Maxwell's equations.

$$\nabla^2\mathbf{H}-\frac{\varepsilon}{c^2}\frac{\partial^2\mathbf{H}}{\partial t^2}=-\frac{4\pi\varepsilon}{c}\nabla\times\left(\frac{\partial}{\partial t}\left(\frac{\mathbf{P}}{\varepsilon}\right)\right)$$

Then further assume for simplicity that $\varepsilon=\varepsilon(y,z)$ is independent of x and expand the magnetic field over the quasi-orthogonal set of the transverse waveguide modes $\mathbf{F_j}$(y,z):

$$\mathbf{H}=\sum_j h_j(x)\mathbf{F}_j(y,z)\mathrm{e}^{ik_j x-i\nu_j t}+\text{c.c.}$$

Here the functions $h_j(x)$ are slowly varying with x, and we can neglect their second derivatives. In general, h_j are also the functions of time, but here we consider the continuous wave operation or pulses that are much longer than all relaxation times in a QCL. The waveguide modes are eigen functions of the equation

$$\varepsilon\left(\frac{\partial}{\partial y}\frac{\partial}{\varepsilon\partial y}+\frac{\partial}{\partial z}\frac{\partial}{\varepsilon\partial z}\right)\mathbf{F}_j+\left(\frac{\omega_j^2\varepsilon}{c^2}-k_j^2\right)\mathbf{F}_j=0$$

The solution of this equation defines both the transverse profile of a given waveguide mode $\mathbf{F_j}$(y,z) and its dispersion, i.e. complex propagation constant $k_j(\nu_j)$ as a function of real frequency of the mode.

Then we have,

$$\sum_j \frac{2ik_j}{\varepsilon}\mathbf{F}_j e^{ik_j x - i\nu_j t}\frac{\partial h}{\partial x} = -\frac{4\pi}{c}\nabla\times\left(\frac{\partial}{\partial t}\left(\frac{\mathbf{P}}{\varepsilon}\right)\right)$$

And assuming the orthogonality condition

$$\int \frac{1}{\varepsilon}F_i F_j^* dA = \delta_{ij} \quad ,$$

where the integration is over the waveguide cross-section and the star denotes complex conjugation. So we have,

$$\frac{\partial h_k}{\partial x} = \frac{2\pi i}{ck_k}e^{-ik_k x + i\nu_k t}\int \nabla\times\left(\frac{\partial}{\partial t}\left(\frac{\mathbf{P}}{\varepsilon}\right)\right)\mathbf{F}_j^* \, dA$$

We recall that the ISB electronic polarization is directed along z axis perpendicular to the QW plane: $\mathbf{P} = P\mathbf{z^0}$. For the waveguide that is sufficiently broad in the y-direction we may also assume that the magnetic field has only y-component. Then:

$$\frac{\partial h_k}{\partial x} = -\frac{2\pi i}{ck_k}e^{-ik_k x + i\nu_k t}\int \frac{1}{\varepsilon}\frac{\partial^2 P}{\partial t \partial x}F_j^* \, dA$$

This equation has to be solved with appropriate boundary conditions on the cavity facets $x = 0$ and $x = L$, taking into account reflection and transmission of the optical power. For a weak signal field, the polarization can be expanded in series in powers of the field, and only the terms of zeroth and first order can be retained. Here

we restrict ourselves to the processes of true lasing, in which the polarization is proportional to the z-component of the electric field of a given mode: $P = \chi E_z$. This would lead to the exponential gain.

The resonant susceptibility χ is a function of all three coordinates x,y,z as it depends on the position of the active layers in a waveguide and the distribution of the drive field intensity across the waveguide and along the cavity. We will, however, assume that the x-dependence of χ is quite smooth and neglect its x-derivative. Then, from the Maxwell's Equations, we have the relation,

$$\frac{\partial^2 P}{\partial t \partial x} \approx -\frac{c\chi}{\varepsilon}\frac{\partial^2 H}{\partial x^2} \approx \frac{c\chi}{\varepsilon}\sum_j h_j k_j^2 F_j e^{ik_j x - i\nu_j t}$$

Suppose that one transverse mode has the excitation threshold considerably lower than all other modes, so there is only one waveguide mode excited. Then we can obtain the equation for the amplitude of this mode:

$$\frac{\partial h}{\partial x} = 2\pi i k h \int \frac{\chi}{\varepsilon^2}|F|^2 dA = \frac{2\pi i \nu \bar{\chi}}{c\mu}\Gamma h$$

where $\Gamma = \mu^2 \int_{\chi \neq 0} \frac{1}{\varepsilon^2}|F|^2 dA$, $\mu = \frac{c\,\mathrm{Re}[k]}{\nu}$ is the effective refractive index of the waveguide mode. Solve this partial deferential equation, it's easy to define the field gain as

$$g_M = \frac{2\pi\nu \,\mathrm{Im}[\chi]}{c\mu}\Gamma$$

and the waveguide loss is $\alpha_w = \mathrm{Im}[k.]$

THEORETICAL RESULTS

Laser gain

Consider the polarization on the Stokes transition 2-3, P_{23}, we have

$$P_{23} = \chi E_3$$

where the χ is the linear resonant susceptibility at the Stokes frequency, E_3 is the electric field generated between transition 2-3, Fig. 9.

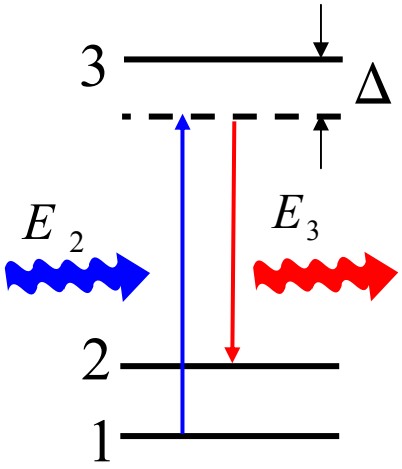

FIG. 9. Stokes transition.

From density matrix equations we can calculate

$$P_{23} = d_{23}\sigma_{32}$$

where σ_{23} is the off-diagonal element, d_{23} is the dipole moment between transition 2-3.

From these two expressions of P_{23}, we can have the relation,

$$\mathrm{Im}[\chi] = (d_{23}/E_3)\mathrm{Im}[\sigma_{32}]$$

The field gain is

$$g_M = \frac{2\pi\nu\,\mathrm{Im}[\chi]}{c\mu}\Gamma$$

So we get the relation between the field gain and the density-matrix element. In order to get the gain of our system, the key point is to find out off-diagonal element of the density-matrix σ_{32}.

For the continuous wave operation that is much longer than all relaxation times, we can neglect the time derivatives in the density-matrix equations. Then the calculation of σ_{32} is reduced to algebra. So we obtain the intensity gain which is double of the field gain,

$$g_I = \frac{4\pi\nu_s d_{32}^2 \Gamma_s}{\hbar c \mu_s}\,\mathrm{Re}\left\{\frac{1}{\Gamma_{32} + \left|\Omega_2\right|^2/\Gamma_{21}^*}\left[\frac{\left|\Omega_2\right|^2 (n_1 - n_3)}{\Gamma_{21}^*\Gamma_{31}^*} - (n_2 - n_3)\right]\right\}$$

where Γ_s is the confinement factor for the Stokes mode. This expression is similar to the one obtained in [5] for the anti-Stokes generation.

Let us analyze this expression for the gain. The gain is not proportional to the Raman inversion $n_1–n_2$ between the initial and final state of the two-photon transition. Instead, there are two terms. Their origin can be seen from inspecting the general structure of density-matrix equations. It is clear that in the absence of the drive field the density matrix element σ_{32} can excited only by the first term on the right-hand side of

$$\frac{d\sigma_{32}}{dt} + \Gamma_{32}\sigma_{32} = i\Omega_3 n_{23} + i\Omega_2 \sigma_{21}^*$$

which is proportional to the Stokes field and the population difference $n_2–n_3$ on the Stokes transition. This term describes linear absorption of the Stokes field on the transition 2-3

After using the experimental parameters taken from reference [1], we use Mathematica to solve the density-matrix equations and expression of gain. We get the curve of gain, varies with the difference

$$\delta = \omega_3 - \omega_{32}$$

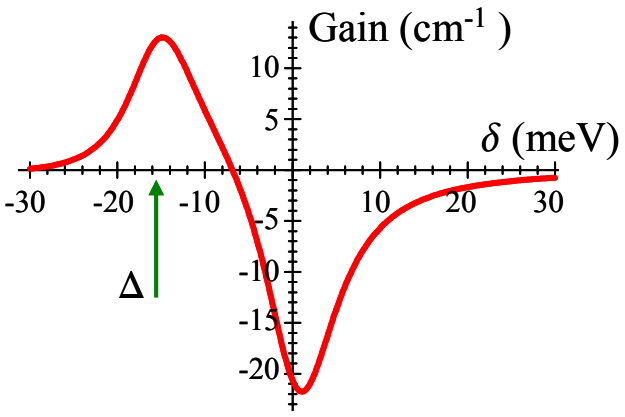

FIG. 10. Gain spectrum for the Stokes field.

From the curve in Fig. 10, the designed value of Δ=15 mev is close to the optimum. That mean Δ is proper to avoid strong first-order absorption and to get the low threshold and high gain.

Losses

The Raman Injection Laser has a heterostructure waveguide which includes hundreds of different layers. However, the active region consists of QW layers that have thickness much smaller than wavelength, so one can average over those layers and use an average complex refractive index of the active region as a whole. As a

result, the waveguide consists of only nine layers.

In reference [6], the wave propagation in multi-layer slab waveguide is discussed. First the wave equation should be derived from Maxwell's equations. Consider the TM mode with the magnetic field polarized transverse to the direction of propagation.

Then by using the technique of separation of variables and the boundary conditions from Maxwell's equations, solutions of these wave equations can be found.

In order to have the guided modes, the fields outside the waveguide core must decay. So we finally obtain the transcendental equation of k from boundary condition.

To solve this kind of equation, computer technique is necessary.

So in our case, from the equation,

$$H = \sum_j h_j(x) F_j(y,z) e^{ik_j x - iv_j t} + c.c.$$

consider, $\mathrm{k} = \mathrm{Re}[\mathrm{k}] + \mathrm{iIm}[\mathrm{k}]$, then we have,

$$H = \sum_j h_j(x) F_j(y,z) e^{-iv_j t} e^{i\,\mathrm{Re}[k_j]x} e^{-\mathrm{Im}[k_j]x} + c.c.$$

We find out the expression of waveguide losses,

$$\alpha_w = \mathrm{Im}[k]$$

This equation would also be:

$$\alpha_w = \mathrm{Im}\left[\frac{\mu v}{c}\right]$$

where $\mu = \frac{c\mathrm{Re}[k]}{v}$ is the effective refractive index of the waveguide mode.

The key point to get the waveguide losses in our system is to find out the complex value of k.

We choose the computer software FEMLab, which is an interactive environment to model single and coupled phenomena based on partial differential equations, as our computer technique.

We simulate the waveguide structure and input the experimental parameters of each layer. Finally the effective refractive index is determined as in Fig. 11. Then we can calculate the waveguide losses.

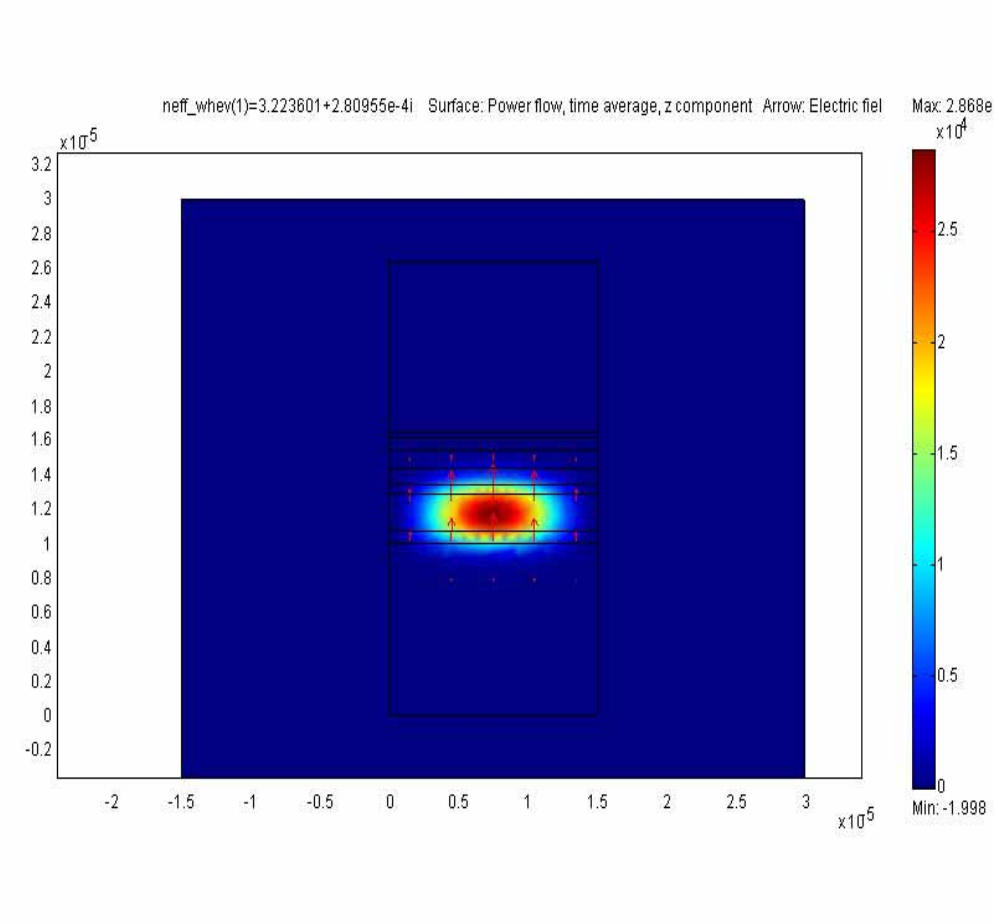

FIG. 11. Waveguide simulation.

Here FEMLab gives the effective refractive index μ=3.223601+i0.000280955.

From equation,

$$\alpha_w = \mathrm{Im}\left[\frac{\mu v}{c}\right]$$

The waveguide losses are around $2\mathrm{cm}^{-1}$.

Power

We know the Poynting Vector represents energy flux density. It's given by: $S = \frac{c}{4\pi} E \times H$. Using the connection between E and H in the TM mode we can have

$$\vec{S} = \frac{c}{4\pi} \vec{E} \times \vec{H} = \frac{c}{4\pi} \sqrt{\frac{\varepsilon}{\mu}} E^2 \cdot \vec{n}$$

So if we can determine the magnitude and distribution of the electric field, we will get the laser output power after integrating over the waveguide cross-section.

To get the power curve, we first solve Maxwell's equations and density-matrix equations to find out the Rabi frequency $\Omega = \frac{d\varepsilon}{2\hbar}$, which is proportional to the electric field. Then after getting the drive electric field e_2 and the Stokes field e_3, the laser power would be proportional to e^2 .

Finally we use reasonable experimental parameters in reference [2]. We take $\eta = 1$, $j_2/j = 0.2$, and T = 10 meV. The total non-resonant cavity losses for the drive and the Stokes modes were taken to be 12 and 13 cm^{-1}, including radiation losses from cavity facets. These numbers correspond to experimentally measured values. As a result, we get the theoretical power curves for drive and Stokes by Mathematica.

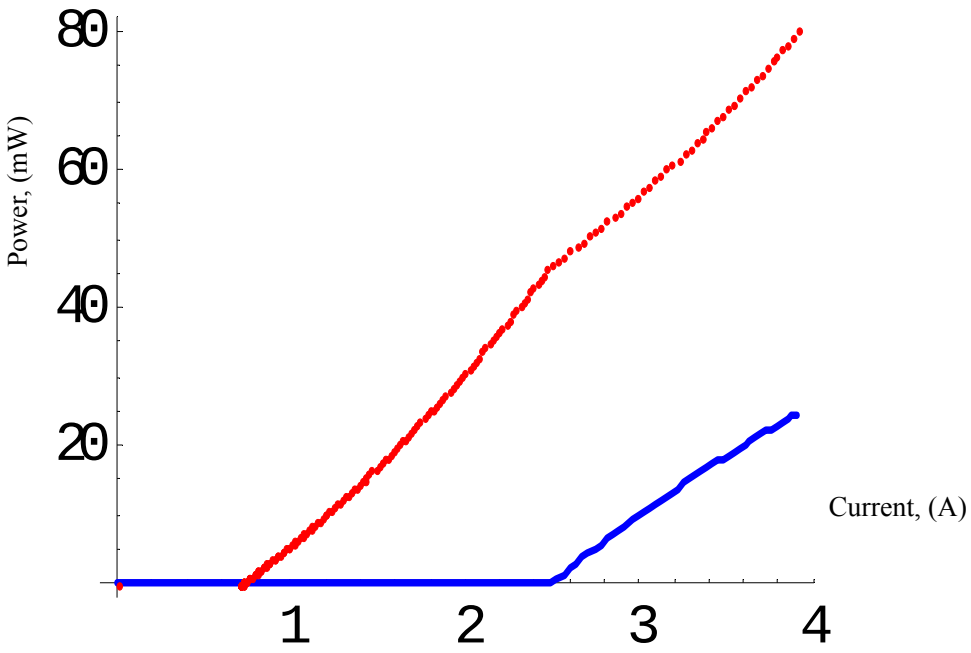

FIG. 12. Theoretical power curve.

In Fig. 12, the red curve is the drive power and the blue curve is the Stokes power. Both of them are plotted as functions of injection current.

In experiment, Raman lasing was reproduced in all ten tested devices. Fourier transform infrared spectrometer was used for optical measurements, together with a calibrated room-temperature HgCdTe detector for the optical power–current characterization. To filter out only the pump laser wavelength in order to measure the optical power emitted at the Stokes frequency, a long-wavelength (7.5mm) pass filter was placed along the light path [1].

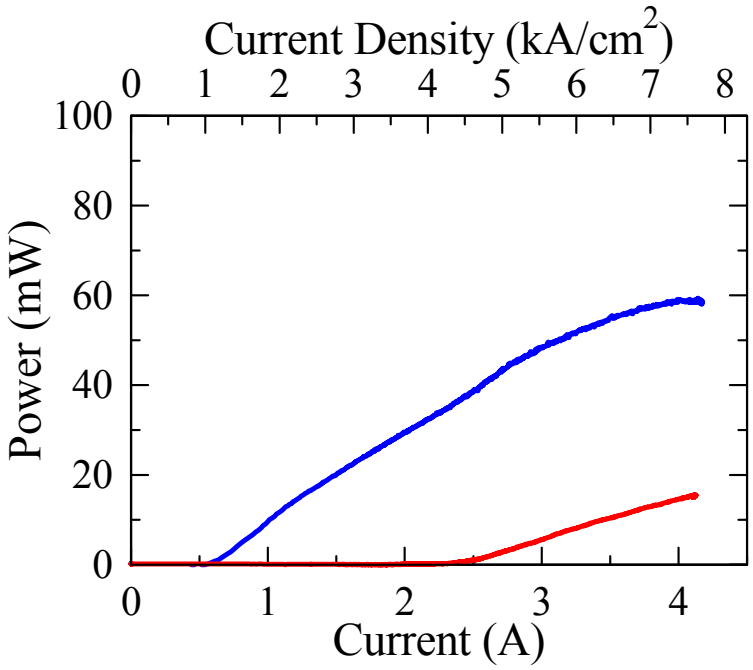

FIG. 13. Experimental power curve.

In Fig. 13, the blue curve is the peak output power for drive emission; the red curve is the Stokes emission. Both curves are measured at temperature of 80 K.

COMPARISON AND CONCLUSION

Compare the calculated plot and measured plot, both the thresholds and the slopes are similar. This proved our theoretical simulations and calculations are correct. Also our anticipation on the design of the Raman Injection Laser is affirmed.

The difference between these two plots is: the slope jumps from high value to low value when the Stokes field turns on in theoretical curve, but it jumps from low value to high value at that point in the experimental curve

This phenomenon can be explained that the slope is much more sensitive to the uncertainties in the input parameters than the laser thresholds.

As the conclusion of this study, the Raman Injection Laser, as a new type of laser, has many benefits like high Raman gain, high conversion efficiency and low threshold compared to the traditional Raman Laser. Also the Raman Injection Laser may have many potential benefits as compared to a standard Quantum Cascade Laser. For example, some benefits which are usually associated with nonlinear optical sources [2]:

1. Generation at frequencies that are not easily accessible for QC lasers in general, or within a given material system;
2. Significantly better tunability and wavelength agility as compared to standard lasers;
3. Higher operating temperature;

4. New functionalities, such as small beam divergence or generation of light with interesting statistical properties

Meanwhile, as compared to the regular Raman lasers, the Raman Injection Laser is much more compact, Fig. 14, have a smaller size and requires a lower power input.

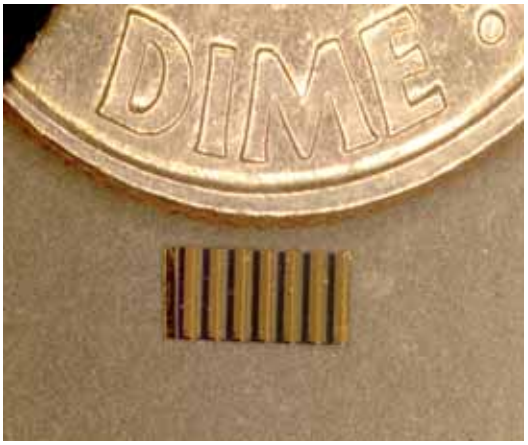

FIG. 14. Small laser size.

REFERENCES

[1] M. Troccoli, A. Belyanin, F. Capasso, E. Cubukcu, D. L. Sivco, et al., Nature **433**, 845 (2005).

[2] A. Belyanin, F. Capasso and M. Troccoli, *Physics and Devices*, (R. Paiella, McGraw-Hill, New York, 2005).

[3] A. Belyanin, D. Liu, F. Xie, F. Capasso and C. Gmachl, *Novel In-Plane Semiconductor Lasers IV*, (edited by C. Mermelstein and D. P. Bour, Proc. SPIE Vol. 5738, 2005), Page 98-108.

[4] A. Belyanin, C. Bentley, F. Capasso, O. Kocharovskaya and M. O. Scully, Phys. Rev. A, **64**, 013814 (2001).

[5] O. Kocharovskaya, Yu. V. Rostovtsev and A. Imamoglu, Phys. Rev. A, **58**, 649 (1998).

[6] H. C. Casey, Jr. and M. B. Panish, *Heterostructure Lasers*, (Academic Press, Orlando, FL, 1978), Page 34-42.

VITA

Debin Liu was born in Chengdu, Sichuan Province, P. R. China in 1981. He received his Bachelor of Science in physics from the University of Science & Technology of China in May 2003. He received the Master of Science in physics from Texas A&M University in August 2005.

Mr. Liu may be reached at Jiaoda 1-8-1-5A, Chengdu, China, 610036. His email address is devinliu@gmail.com.